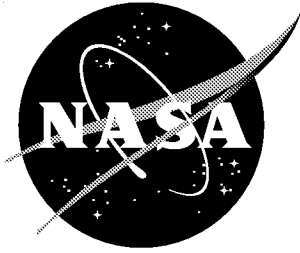


NASA/TP-2001-211272



The Langley Parameterized Shortwave Algorithm (LPSA) for Surface Radiation Budget Studies

Version 1.0

*Shashi K. Gupta
Analytical Services and Materials, Inc., Hampton, Virginia*

*David P. Kratz and Paul W. Stackhouse, Jr.
Langley Research Center, Hampton, Virginia*

*Anne C. Wilber
Analytical Services and Materials, Inc., Hampton, Virginia*

December 2001

The NASA STI Program Office ... in Profile

Since its founding, NASA has been dedicated to the advancement of aeronautics and space science. The NASA Scientific and Technical Information (STI) Program Office plays a key part in helping NASA maintain this important role.

The NASA STI Program Office is operated by Langley Research Center, the lead center for NASA's scientific and technical information. The NASA STI Program Office provides access to the NASA STI Database, the largest collection of aeronautical and space science STI in the world. The Program Office is also NASA's institutional mechanism for disseminating the results of its research and development activities. These results are published by NASA in the NASA STI Report Series, which includes the following report types:

- **TECHNICAL PUBLICATION.** Reports of completed research or a major significant phase of research that present the results of NASA programs and include extensive data or theoretical analysis. Includes compilations of significant scientific and technical data and information deemed to be of continuing reference value. NASA counterpart of peer-reviewed formal professional papers, but having less stringent limitations on manuscript length and extent of graphic presentations.
- **TECHNICAL MEMORANDUM.** Scientific and technical findings that are preliminary or of specialized interest, e.g., quick release reports, working papers, and bibliographies that contain minimal annotation. Does not contain extensive analysis.
- **CONTRACTOR REPORT.** Scientific and technical findings by NASA-sponsored contractors and grantees.

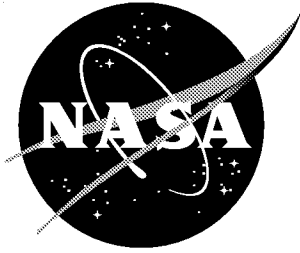
- **CONFERENCE PUBLICATION.** Collected papers from scientific and technical conferences, symposia, seminars, or other meetings sponsored or co-sponsored by NASA.
- **SPECIAL PUBLICATION.** Scientific, technical, or historical information from NASA programs, projects, and missions, often concerned with subjects having substantial public interest.
- **TECHNICAL TRANSLATION.** English-language translations of foreign scientific and technical material pertinent to NASA's mission.

Specialized services that complement the STI Program Office's diverse offerings include creating custom thesauri, building customized databases, organizing and publishing research results ... even providing videos.

For more information about the NASA STI Program Office, see the following:

- Access the NASA STI Program Home Page at <http://www.sti.nasa.gov>
- E-mail your question via the Internet to help@sti.nasa.gov
- Fax your question to the NASA STI Help Desk at (301) 621-0134
- Phone the NASA STI Help Desk at (301) 621-0390
- Write to:
NASA STI Help Desk
NASA Center for Aerospace Information
7121 Standard Drive
Hanover, MD 21076-1320

NASA/TP-2001-211272



The Langley Parameterized Shortwave Algorithm (LPSA) for Surface Radiation Budget Studies

Version 1.0

*Shashi K. Gupta
Analytical Services and Materials, Inc., Hampton, Virginia*

*David P. Kratz and Paul W. Stackhouse, Jr.
Langley Research Center, Hampton, Virginia*

*Anne C. Wilber
Analytical Services and Materials, Inc., Hampton, Virginia*

National Aeronautics and
Space Administration

Langley Research Center
Hampton, Virginia 23681-2199

December 2001

Available from:

NASA Center for AeroSpace Information (CASI)
7121 Standard Drive
Hanover, MD 21076-1320
(301) 621-0390

National Technical Information Service (NTIS)
5285 Port Royal Road
Springfield, VA 22161-2171
(703) 605-6000

Preface

A research effort for surface radiation budget (SRB) studies was initiated at the NASA Langley Research Center (LaRC) in the mid-1980's with the goal of developing parameterized, fast radiative transfer algorithms for deriving shortwave (SW) and longwave (LW) components of SRB on a global scale using meteorological products from operational satellites. During the ensuing years, a group of scientists at the LaRC developed SW and LW algorithms and derived global fields of all components of SRB. The product of this effort was the first long-term global dataset of SRB components based on satellite data. This dataset has since been published and made available to the climate science community.

The SW algorithm for the above effort was developed by W. F. Staylor (with help from W. L. Darnell and the first author of this report), and came to be known as the Staylor algorithm. Staylor accounted for extinction of solar radiation in the atmosphere by adopting existing parameterizations from the literature for some processes, modifying existing ones for others, and developing new ones for still others. The early versions of this algorithm used meteorological products from the TIROS Operational Vertical Sounder (TOVS) and the Advanced Very High Resolution Radiometer (AVHRR) flown aboard NOAA's operational satellites, and were fine-tuned using surface insolation measurements from a number of sites in the U. S. Later versions were adapted to use meteorological data and other inputs from the International Satellite Cloud Climatology Project (ISCCP) and the Earth Radiation Budget Experiment (ERBE), and were extensively validated with surface measurements from the Global Energy Balance Archive (GEBA) and other sources.

Despite its simplicity and computational efficiency, this SW algorithm performed remarkably well when compared with much more detailed and computationally slower algorithms. It compared favorably in the InterComparison of Radiation Codes in Climate Models (ICRCCM) and other validation exercises sponsored by the World Climate Research Program (WCRP). This led to its selection by the WCRP/SRB project in the early 1990's as one of the two algorithms for producing global insolation datasets. It was also selected by the Global Energy and Water-cycle Experiment (GEWEX)/SRB Workshop in 1993 as a quality-check algorithm for monitoring the performance of the primary algorithm chosen by the GEWEX/SRB project. Currently, it is being tested by the NASA/Clouds and the Earth's Radiant Energy System (CERES) project along with other surface SW algorithms. There is considerable interest on the part of the CERES project in using this algorithm for deriving surface SW products.

Along with the strengths mentioned above, this algorithm suffered from a number of serious weaknesses. Generally, the sources of information used were not well documented. Parameterizations supposedly taken from the literature were difficult to trace to their referenced sources. The assumptions and approximations made in the algorithm were not adequately explained or justified. Seemingly complicated formulas developed for the algorithm were not supported by a satisfactory analytical framework. These shortcomings often resulted in less than enthusiastic acceptance and use of this algorithm by the scientific community.

Despite the noted shortcomings, superior performance of this algorithm sustained the interest of the GEWEX/SRB and CERES projects in its continued use. To meet the needs of these projects, another effort was undertaken at LaRC to fully document the scientific basis of this algorithm. Efforts were made to relate the information taken from the literature to its original sources, clarify and justify the assumptions and approximations used, and establish the analytical framework for the formulas developed and used. Changes were made when some components of the algorithm could not be justified. Also, a fully documented FORTRAN-90/95 code was developed for implementing this algorithm using newer sources of meteorological inputs and providing results at higher spatial resolution. The present report represents the first step of the latter effort. Having undergone large-scale changes during this process, and

with many more changes on the way to meet the future needs of the new projects, this algorithm needed a new identity. It has been renamed the Langley Parameterized Shortwave Algorithm (LPSA).

Acknowledgments

The cause of documenting and restructuring this algorithm has greatly benefited from the earlier efforts of two individuals. Charles Whitlock, who directed the WCRP/SRB activity at the LaRC, expended considerable effort on documenting this algorithm in his reports to the WCRP. The authors have gathered much information from his reports and through personal consultations with him. Nancy Ritchey worked with W. F. Staylor through much of the development of this algorithm and developed most of the computer code (along with one of the present authors, Anne Wilber) for its implementation. Her internal documentation of the code has been a valuable source of information. Also, Whitlock, Ritchey, and Gary Gibson have generously given of their time to critically review this report and make valuable suggestions for improvement. The authors owe a debt of gratitude to all three.

1. Introduction and background

The surface radiation budget (SRB) is a major component of the energy exchange between the atmosphere and the land/ocean surface and thus exercises a profound influence on many weather and climate processes (Ramanathan 1986). Developing a long-term climatology of SRB on a global scale was recognized as an essential prerequisite for a number of World Climate Research Program (WCRP) research projects (Suttles and Ohring 1986). In response, the WCRP established the SRB Climatology Project (WCRP-69 1992) to facilitate and monitor the development of a reliable long-term climatology of SRB. Recognition of the scientific potential of SRB also led to the creation of a SRB program at the NASA Langley Research Center (LaRC) starting in mid-1980's. The main objective of the LaRC program was to develop efficient algorithms for producing SRB parameters on a global scale, preferably using input data from operational satellite sources.

The algorithm for deriving surface SW fluxes for the LaRC program was developed by W. F. Staylor and colleagues (Staylor et al. 1983; Darnell et al. 1988, 1992), and became known as the Staylor algorithm. Meteorological products from NOAA's polar-orbiting satellites were chosen as inputs for the algorithm because of their global coverage. The first version of this algorithm used water vapor and ozone abundances from TOVS data products. Planetary albedos derived from AVHRR data were used as proxy for cloud parameters. The second version was tailored to take advantage of the C1 datasets as those became available from ISCCP (Rossow and Schiffer 1991). Cloud products derived from the ISCCP network of geostationary satellites, intercalibrated with AVHRR data taken from one or two polar platforms, resulted in a much improved SRB dataset from the second version. A global SRB climatology derived using the second version and the entire 8-year record of ISCCP-C1 data (July 1983 to June 1991) has been published recently (Gupta et al. 1999). Also, this dataset has been made available online to the science community worldwide from the LaRC Atmospheric Sciences Data Center (<http://eosweb.larc.nasa.gov>).

The purpose of this report is to present a new version of the Staylor algorithm with detailed description and documentation of its methodology. Also, a FORTRAN-90/95 code has been developed for the implementation of the new version. Section 2 identifies the limitations of the older versions and makes a case for restructuring the algorithm for newer applications. Section 3 examines the simple basis of the algorithm and links that basis, wherever possible, to its original sources in the literature. Section 4 describes the sources of input data used in the past, in use at present, and being considered for the future. A complete list of surface SW parameters and sample results derived from the new version are presented in Sec. 5. A short list of planned enhancements is presented in Sec. 6.

2. Case for restructuring

The Staylor algorithm is simple, computationally efficient, and above all, provides good results. Its potential remains largely unrealized, however, because it has not been accepted widely by the science community. It is not difficult to identify the reasons for this non-acceptance, the foremost being the lack of detailed documentation of the methodology. In some cases, material referenced from literature sources was not traceable to those sources, or the assumptions and approximations used were not sufficiently explained or justified. In other cases, complex formulas developed for the algorithm were not supported by an adequate analytical framework. It became obvious that such conditions had to be remedied before this algorithm and its results would gain wider acceptance.

There are a number of other reasons which motivated the development of the new version of this algorithm. Based on its superior performance, the WCRP/SRB (same as the GEWEX/SRB) project had designated it as the quality-check algorithm for monitoring the performance of the primary SW algorithm developed by Pinker and Laszlo (1992a). The GEWEX/SRB project is required to produce surface fluxes on a $1^\circ \times 1^\circ$ spatial resolution using meteorological inputs from data assimilation models. Cloud

parameters for the GEWEX/SRB project are being produced on a $1^\circ \times 1^\circ$ spatial grid using pixel-level (DX) data from ISCCP (Stackhouse et al. 2000). The CERES project at NASA/LaRC currently produces net SW fluxes at the surface using satellite-derived top-of-atmosphere (TOA) broadband SW fluxes with the TOA-to-surface transfer algorithm developed by Li et al. (1993). Validation of net SW fluxes is difficult to accomplish because the most commonly measured surface SW parameter is insolation. Algorithms for converting net SW flux to insolation are of limited use because they require prior knowledge of surface albedo fields. As a result, there is interest in the CERES project in using this algorithm for producing surface insolation independently of the Li et al. algorithm. Continued interest by the GEWEX/SRB and CERES projects in the use of this algorithm necessitated the development of a well-documented and scientifically justifiable version. This new version has been named the Langley Parameterized Shortwave Algorithm (LPSA).

3. The algorithm

On a very basic level, surface insolation (downward SW flux at the surface), F_{SD} , in the LPSA is computed as

$$F_{SD} = F_{TOA} T_A T_C, \quad (1)$$

where F_{TOA} is the corresponding insolation at the TOA, T_A is the transmittance of the clear atmosphere, and T_C is the transmittance of clouds. All quantities in Eq. (1) refer to the broadband SW region, approximately from 0.3 to 5.0 μm . The temporal resolution of the current version of LPSA is daily, i.e. all parameters are computed on a daily average basis.

3.1. TOA insolation

F_{TOA} is computed as (Peixoto and Oort 1993)

$$F_{TOA} = S (d_m / d)^2 \cos Z, \quad (2)$$

where:

S - solar constant,

d - instantaneous Sun-Earth distance,

d_m - mean Sun-Earth distance, also called the astronomical unit, and

Z - solar zenith angle.

The value of $\cos Z$ for any location and time is computed as

$$\cos Z = \sin \phi \sin \delta + \cos \phi \cos \delta \cos h, \quad (3)$$

where ϕ is the latitude of the location, δ is the solar declination at the time, and h is the hour angle (in radians) from the local meridian. For a more detailed definition of h , the reader is referred to Sellers (1965). A few simple relationships that follow from Eq. (3), and will be of interest later, are presented below. At sunrise and sunset, $Z = \pi/2$, and $h = H$ (defined as half day length), so that

$$\sin \phi \sin \delta + \cos \phi \cos \delta \cos H = 0, \quad (4)$$

which gives

$$\cos H = -\tan \delta \tan \phi, \quad (5)$$

or

$$H = \cos^{-1}(-\tan \delta \tan \phi). \quad (6)$$

The eccentricity correction parameter, $(d_m/d)^2$, and the solar declination, δ , are both functions of time. Strictly speaking, Eqs. (2) and (3) used for computing F_{TOA} are applicable only on an instantaneous basis. In the current work, however, simple expressions presented by Iqbal (1983) for computing daily average values of $(d_m/d)^2$ and δ were used to match the daily temporal resolution of the algorithm. A brief discussion of those expressions and the maximum errors of daily average values computed with them is presented in Appendix A. The maximum error incurred in computing F_{TOA} using daily averages instead of instantaneous values of $(d_m/d)^2$ and δ was estimated to be less than 0.01%.

Daily total insolation at the TOA, FD_{TOA} , can be computed by integrating Eq. (2) from sunrise to sunset as

$$FD_{TOA} = S (d_m/d)^2 \int_{sunrise}^{sunset} \cos Z dt. \quad (7)$$

When time is measured in hours,

$$dt = \frac{12}{\pi} dh, \quad (8)$$

and

$$FD_{TOA} = \frac{24}{\pi} S (d_m/d)^2 \left(\int_0^H \sin \delta \sin \phi dh + \int_0^H \cos \delta \cos \phi \cos h dh \right), \quad (9)$$

Integrating Eq. (9) gives

$$FD_{TOA} = \frac{24}{\pi} S (d_m/d)^2 (H \sin \delta \sin \phi + \cos \delta \cos \phi \sin H), \quad (10)$$

and hourly average TOA insolation, FDA_{TOA} as

$$FDA_{TOA} = \frac{1}{\pi} S (d_m/d)^2 (H \sin \delta \sin \phi + \cos \delta \cos \phi \sin H), \quad (11)$$

averaged over a 24-hour day.

Staylor computed daily average TOA insolation in terms of a parameter D , defined as

$$D = \frac{1}{\pi} \left\{ F \cos^{-1}(-F/G) + G \sqrt{1 - (F/G)^2} \right\}, \quad (12)$$

where $F = \sin \delta \sin \phi$, and $G = \cos \delta \cos \phi$. Equation (12) is the same as Eq. (11) without the Sun-Earth distance corrected solar constant, $S (d_m/d)^2$. Staylor named the parameter D as the daily mean vertical Sun fraction. D is the ratio of the actual daily TOA insolation to that if the Sun was overhead for the entire 24

hours. D can also be viewed as the value of $\cos Z$ averaged over the 24-hour day. Staylor also defined another parameter, u , as the average of $\cos Z$ from sunrise to sunset (Staylor and Wilber 1990), in the form

$$u = F + G \sqrt{(G \mp F)/2G}. \quad (13)$$

The authors were not able to derive an expression for u in the form shown in Eq. (13). It was decided, therefore, to derive an expression for u from first principles as

$$u = \frac{1}{\text{day length}} \int_{\text{sunrise}}^{\text{sunset}} \cos Z \, dt, \quad (14)$$

where ‘day length’ represents the time from sunrise to sunset in hours. Equation (14) can also be written in terms of F , G , and h as

$$u = \frac{1}{H} \int_0^H (F + G \cos h) \, dh = F + \frac{G \sin H}{H}, \quad (15)$$

or

$$u = \frac{F \cos^{-1}(\mp F/G) + G \sqrt{1 \mp (F/G)^2}}{\cos^{-1}(\mp F/G)}. \quad (16)$$

The values of u computed with Eqs. (13) and (16) were found to be significantly different. The highest value of u which occurs at the equator during the equinoxes was found to be 0.707 for Eq. (13) and 0.637 for Eq. (16). The parameter u was extensively used by Staylor for deriving approximate values of a number of input variables (e.g., see Eqs. 39, 42, 43, 46, and 49) which are known to be dependent on Z (or $\cos Z$). These input variables were essential for computing insolation but were not always available for all conditions from their regular sources. This strategy proved valuable in eliminating large gaps in the computed flux fields when those input variables were not available.

Equations (12) and (16) for D and u respectively, apply over most of the globe where there is sunrise and sunset during the course of a day, and $-1 \leq F/G \leq 1$. Over polar regions of the summer hemisphere, there is no sunset, $F/G > 1$, and

$$\cos^{-1}(\mp F/G) = H = \pi. \quad (17)$$

The term $G \sqrt{1 \mp (F/G)^2}$ in Eqs. (12) and (16) becomes undefined. At those latitudes,

$$D = u = F. \quad (18)$$

Over polar regions of the winter hemisphere, there is no sunrise, $F/G < -1$, both D and u are undefined and are set equal to zero.

3.2. Clear-sky transmittance

Clear-sky transmittance, T_A , was computed as

$$T_A = (1 + B) e^{-\tau_z}, \quad (19)$$

where B is a backscatter term (defined later in Eq. 33), τ_z is the broadband extinction optical depth at solar zenith angle Z and accounts for all absorption and scattering processes in the clear atmosphere. Staylor analyzed clear-sky insolation measurements from several sites within the United States to empirically derive the dependence of τ_z on Z in the form

$$\tau_z = \tau_0 (\sec Z)^N, \quad (20)$$

where τ_0 is the broadband optical depth for overhead Sun (Darnell et al. 1992). In first two versions of the algorithm, an expression for the exponent N was derived empirically in the form

$$N = 1.1 \square 2.0 \tau_0. \quad (21)$$

Another method, to be presented later in this section, is being used for deriving N in the current version of the algorithm.

The vertical optical depth (for overhead Sun), τ_0 , was computed as

$$\tau_0 = -\ln(1 - \alpha_0), \quad (22)$$

where α_0 is an effective vertical attenuation factor for broadband radiation. Functionally, α_0 is the equivalent of an absorptance, and may be called an ‘extinctance.’ Staylor computed α_0 in terms of effective attenuation factors for the many absorbing/scattering constituents of the clear atmosphere as

$$\alpha_0 = \alpha_{H_2O} + \alpha_{O_3} + \alpha_{CO_2} + \alpha_{O_2} + \alpha_{Ray} + \alpha_{Aer}, \quad (23)$$

where the first four terms on the right represent attenuation by the respective absorbing gases, α_{Ray} represents attenuation due to Rayleigh scattering, and α_{Aer} , the attenuation due to aerosols. Staylor’s choice of this formulation was guided by the fact that all attenuation factors except α_{Aer} were already available in the literature. Note that the addition of individual attenuation terms as shown in Eq. (23) is justifiable only if the processes represented by them occur independently of one another. In simple terms, it means that either these processes occur in different regions of the spectrum, or in different altitude ranges of the atmosphere. Among the processes dominating the extinction of solar radiation in the Earth’s atmosphere, absorption by ozone takes place in the ultraviolet and visible regions and primarily in the stratosphere. Rayleigh scattering also occurs in the ultraviolet and the visible but mostly in the troposphere. Water vapor absorption takes place in the near infrared and in the troposphere. These processes may be considered independent of one another in accordance with the above requirement. The remaining extinction processes are much less significant.

Staylor used the following formulas to represent attenuation factors for the various processes:

$$\square_{H_2O} = 0.100 (U_{H_2O})^{0.27}, \quad (24)$$

$$\square_{O_3} = 0.037 (U_{O_3})^{0.43}, \quad (25)$$

$$\square_{CO_2} = 0.006 \left(P_S \frac{350}{300} \right)^{0.29}, \quad (26)$$

$$\square_{O_2} = 0.0075 (P_S)^{0.87}, \quad (27)$$

and

$$\square_{Ray} = 0.035 (P_S)^{0.67}, \quad (28)$$

where U_{H_2O} represents the column water vapor amount (in precipitable cm), U_{O_3} , the column ozone amount (in cm-atm), and P_S , the surface pressure (in atm). These formulas have changed only slightly between evolving versions of the algorithm. The attenuation factors in Eqs. (26) – (28) are tied to the surface pressure which acts as a surrogate for column abundances of the uniformly mixed gases. The fraction (350/300) in Eq. (26) represents a scaling of CO₂ attenuation to the present-day mixing ratio of 350 ppm from the 300 ppm most likely used in the original formula. Equation (27) above was taken from the first version of the algorithm (Darnell et al. 1988) even though 0.002 (in place of 0.0075) appeared in later versions. The form of Eq. (27) given above matches exactly with the formula for O₂ absorption given by Hoyt (1978). Staylor attributed attenuation factors of Eqs. (24), (25), and (28) to Lacis and Hansen (1974), and those of Eqs. (26) and (27) to Yamamoto (1962). An examination of the above papers shows that formulas in the forms as in Eqs. (24) – (28) are not presented in those papers. A closer examination of Eqs. (24) – (28), and their relationships and comparisons with the material contained in those papers is presented in Appendix B.

The formula used for \square_{Aer} in the current version of the algorithm has the form

$$\square_{Aer} = \square_{Aer} (1 - \omega_0) + \frac{1}{2} \square_{Aer} \omega_0 (1 - g), \quad (29)$$

where \square_{Aer} , ω_0 , and g are the broadband aerosol optical depth, single scattering albedo, and asymmetry parameter, respectively. The first term on the right represents attenuation by aerosol absorption, and the second term, by aerosol backscattering (Wiscombe and Grams 1976). Forward scattering by aerosols does not cause attenuation of the downward radiation stream and, therefore, is not included in Eq. (29). It is noted that Staylor did not use ω_0 in the second term assuming ω_0 to be always close to unity. The lowest value of ω_0 used by Staylor (for continental aerosol, see Appendix C) was 0.90. Information on the geographical distribution and radiative properties of aerosols used in the current work is presented in Appendix C. Also, for the sake of completeness, it needs to be mentioned that in earlier versions (Darnell et al. 1992), the formula for \square_{Aer} had the form

$$\square_{Aer} = 0.007 + 0.009 (U_{H_2O}), \quad (30)$$

which tied \square_{Aer} to the moisture content of the atmosphere.

The value of the exponent N of Eq. (20) for the current version was derived using \square_{Aer} computed at

two values of Z . $Z = 0^\circ$ and 70.5° were chosen to cover a wide range. Corresponding values of $\bar{\tau}$ are denoted as $\bar{\tau}_b$ and $\bar{\tau}_{70}$. $\bar{\tau}_0$ was computed from Eq. (23), and $\bar{\tau}_b$ thereafter from Eq. (22). Values of $\bar{\tau}_{70}$ and $\bar{\tau}_0$ were computed by substituting 3 times the constituent abundances in Eqs. (24) – (29) and then applying Eqs. (23) and (22). Note that for $Z = 70.5^\circ$, $\sec Z$, which represents the relative air mass is equal to 3. Finally, from Eq. (20)

$$\bar{\tau}_{70} = \bar{\tau}_b (\sec Z)^N = \bar{\tau}_b (3)^N, \quad (31)$$

which gives

$$N = \frac{1}{\ln 3} \left\{ \ln(\bar{\tau}_{70}) - \ln(\bar{\tau}_b) \right\}, \quad (32)$$

providing an average value of N for the entire range of Z from 0° to 70.5° .

The term B introduced in Eq. (19), represents radiation backscattered by the atmosphere after being reflected upward from the surface. It represents an enhancement of the downward radiation stream and currently has the form

$$B = 0.065 P_S A_S + 2 A_S \bar{\tau}_{Aer} \bar{\tau}_0 (1 - g), \quad (33)$$

where A_S is the surface albedo. The first term on the right represents the Rayleigh backscattering of the surface reflected (diffuse) radiation. The value of the coefficient in the first term (0.065) is in good agreement with the estimate of spherical albedo of a Rayleigh atmosphere illuminated from below (Lacis and Hansen 1974). The second term represents the surface reflected radiation backscattered by aerosols. In this term also, Staylor did not use $\bar{\tau}_0$ for the same reason as stated in connection with the second term of Eq. (29). Note that the magnitude of this enhancement in Eq. (33) is four times larger than the attenuation by a similar process represented by the second term in Eq. (29). This is a result of two causes: i) the surface reflected radiation is completely diffuse and the scattering optical depth for diffuse radiation is approximately double that for the direct radiation (Wiscombe and Grams 1976), and ii) the reflected radiation makes two passes through the atmosphere doubling the scattering optical depth again. Note further that the aerosol term was not included in the expression for B in the first two versions of the algorithm. In the second version (Darnell et al. 1992), only the first term on the right in Eq. (33) was used to represent B . Prior to that, in the first version (Darnell et al. 1988), the backscattering enhancement was included as a negative term ($-0.065 P_S A_S$) in the expression for $\bar{\tau}_0$ in Eq. (23).

3.3. Cloud transmittance

Cloud transmittance, T_C , for a grid box was computed in terms of visible reflectances as

$$T_C = 0.05 + 0.95 \frac{(R_{ovc} - R_{meas})}{(R_{ovc} - R_{clr})}, \quad (34)$$

where R_{ovc} , R_{clr} , and R_{meas} represent daily average values of overcast, clear, and measured reflectances respectively corresponding to an overhead Sun. Values of R_{meas} were computed by averaging measured daytime instantaneous (3-hourly) reflectances, weighted by μ_0 , the instantaneous value of $\cos Z$. Equation (34) is based on standard threshold methods used for cloud parameter determination (e.g., Moser and Raschke 1984) and a recognition of the observational fact that even for the thickest clouds, T_C is not reduced to zero.

Since completely overcast conditions do not occur every day, R_{ovc} was computed using a regression relation of the form

$$R_{ovc} = \frac{C_1}{\mu \mu_o} + \frac{C_2}{\mu \mu_o} \left[\frac{\mu \mu_o}{(\mu + \mu_o)} \right]^2, \quad (35)$$

where μ is the cosine of the instantaneous view zenith angle. Coefficients C_1 and C_2 were determined off-line, separately for each ISCCP satellite for every month, by linear regression between $R_{ovc}\mu\mu_o$ and $[\mu\mu_o/(\mu+\mu_o)]^2$. The theoretical basis for Eq. (35) can be found in Staylor (1985). Reflectances used in the above regression were sampled from the monthly ensemble of overcast reflectances on the basis of cloud optical depths. Only reflectances corresponding to the highest 10 – 20% range of cloud optical depth values were selected.

At least two different methods were used for computing the values of R_{clr} depending on the underlying surface type. For ice-free ocean surface, R_{clr} was computed from

$$R_{clr} = C_3 + C_4 (\mu \mu_o)^{0.75}. \quad (36)$$

Information on the theoretical basis of Eq. (36) was not available. Coefficients C_3 and C_4 were also determined for each ISCCP satellite for every month by linear regression between sampled daily averages of R_{clr} and $(\mu\mu_o)^{0.75}$ for clear-sky grid boxes over ice-free ocean. An alternative method was used for all surface types other than ice-free ocean. With this method, R_{clr} for each grid box was computed by averaging all available daytime values of clear-sky visible reflectance. The authors note that even though different methods of computing R_{clr} were suggested in Darnell et al. (1992) for different surface types (e.g., land, snow-covered land), only the method described in this paragraph was implemented in the code. Details of the sampling procedures used for both regression analyses (Eqs. 35 and 36) are presented in Appendix D.

It should be noted that the use of Eq. (34) was not found to be appropriate for all grid boxes and all days. Under certain conditions, other methods for computing T_C had to be used. A discussion of the conditions under which alternative computation of T_C was necessary and the equations used for those computations is also presented in Appendix D.

3.4. Surface albedo

Surface albedo, A_S , is an important SRB parameter as the primary determinant of net or absorbed SW radiation, F_{SN} , which is computed as

$$F_{SN} = F_{SD} (1 - A_S). \quad (37)$$

On a secondary level, surface albedo also affects the downward SW radiation through the backscattered radiation term represented by Eq. (33). The all-sky surface albedo used in Eq. (37) was computed by Staylor as

$$A_S = A_{Sovc} + (A_{Sclr} - A_{Sovc}) T_C^2, \quad (38)$$

where A_{Sclr} and A_{Sovc} represent surface albedos for clear-sky and overcast conditions respectively. A_{Sclr} and A_{Sovc} may be substantially different because of the differences between illumination geometry under clear-sky and overcast conditions. Staylor obtained A_{Sclr} and A_{Sovc} from different sources for different surface types as described below.

Ice-free oceans: For ice-free oceans, Staylor (Darnell et al. 1992) computed surface albedos as

$$A_{Sclr} = 0.039 / u, \quad (39)$$

and

$$A_{Sovc} = 0.065. \quad (40)$$

Even though Darnell et al. (1992) refer to Payne (1972) and Kondratyev (1973) as the sources of Eq. (39), an equation of this form is not found in those documents. Closer examination of those documents shows, however, that the results reported therein agree with those represented by Eqs. (39) and (40). The authors believe that Staylor developed Eq. (39) in its simple form using results reported in Payne (1972) and Kondratyev (1973). Darnell et al. (1992) also showed that Eq. (40) follows from Eq. (39) for $u = 0.60$, which in turn, corresponds to $Z = 53^\circ$. Note that 53° represents a good estimate of an effective value of Z for diffuse radiation.

Other snow/ice-free surfaces: For all snow/ice-free surfaces other than ice-free ocean, Staylor used surface albedos derived from monthly-average clear-sky TOA albedos obtained from the Earth Radiation Budget Experiment (ERBE; Barkstrom et al. 1989). ERBE-based surface albedos were used whenever and wherever they were available, and were derived as described below. Linear relationships between clear-sky TOA albedo, A_{Tclr} , and corresponding surface albedo have been developed over the years in the simple form

$$A_{Tclr} = a + b A_{Sclr}, \quad (41)$$

(e.g., Chen and Ohring 1984; Koepke and Kriebel 1987), generally on an instantaneous basis. The constants a and b represent the effect of the intervening atmosphere and are functions of the atmospheric properties. Staylor (see Staylor and Wilber 1990) adapted Koepke and Kriebel's version of Eq. (41) for daily average values of A_{Tclr} and A_{Sclr} . This version includes the effects of Rayleigh scattering, water vapor, ozone, and aerosols built into the constants a and b . For the daily average form of Eq. (41), Staylor and Wilber (1990) represented the above constants as

$$a = 0.25 P_s / (1 + 5u), \quad (42)$$

and

$$b = 1 - a - 0.04 \left\{ 16 U_{O_3} / (1 + 5u) \right\}^{0.6} - 0.12 (U_{H_2O})^{0.25} - 2.4 \Delta_{Aer} (1 - \Delta_0) u^{0.4} - \Delta_{Aer} / (2 + 15 u^{1.5}), \quad (43)$$

and computed the value of A_{Sclr} as

$$A_{Sclr} = (A_{Tclr} - a) / b. \quad (44)$$

Note that expressions for a and b as given in Eqs. (42) and (43) were not found in either Chen and Ohring (1984) or Koepke and Kriebel (1987). Also, in earlier versions of the algorithm (see Darnell et al. 1992), a simpler relationship of the form

$$A_{Sclr} = 1.3 A_{Tclr} - 0.07, \quad (45)$$

was used which was based primarily on the work of Chen and Ohring (1984).

Monthly average clear-sky TOA albedos (A_{Tclr}) from ERBE were available for a period of 51 months from March 1985 to May 1989. Corresponding monthly average values of A_{Sclr} for these months were computed from Eq. (44) and used as such for every day of the respective months. The possibility of using ERBE-derived values of A_{Sclr} for months outside the ERBE period was also examined. To that end, interannual variability of ERBE-derived A_{Sclr} for each month over the available years was analyzed. This analysis showed interannual variability of up to 10% over high and mid latitudes of the Northern Hemisphere (NH), and in the 1 – 2% range over lower latitudes and most of the Southern Hemisphere (SH). Staylor, therefore, decided to use multi-year averages of A_{Sclr} for each month from the ERBE period, for corresponding months outside the ERBE period. This practice is being continued until better surface albedo datasets become available. For all snow/ice-free regions where ERBE-derived A_{Sclr} was used, A_{Sovc} was derived from

$$A_{Sovc} = 1.1 A_{Sclr} u^{0.2}. \quad (46)$$

Surfaces affected by snow/ice: Staylor also made use of ERBE-derived surface albedos for regions which were affected by snow/ice. For such regions, however, ERBE-derived values were modified to account for the presence of snow/ice. When ERBE-derived values were not available for some snow/ice affected regions, Staylor devised other relationships for deriving surface albedos using snow/ice fractional cover for that region and completed the flux calculation. The forms of those relationships and the conditions under which they were used are discussed in Appendix E.

It is important to note here that Staylor’s choice of Eqs. (39) and (40) over oceans, and ERBE-based surface albedos over other regions helped overcome a serious difficulty in deriving broadband SW fluxes. These albedos were already broadband. Attempts to derive broadband surface albedos from ISCCP visible radiances were plagued with large uncertainties involved in the narrowband-to-broadband conversion.

3.5. Direct, diffuse, and PAR

Direct and diffuse broadband fluxes, and PAR (photosynthetically active radiation, between 0.4 and 0.7 μm) are components of global insolation which are important for a variety of applications. Staylor devised simple formulas for partitioning global flux into direct and diffuse components based primarily on cloud transmittance, T_C . Specifically, the partitioning formulas depended on whether or not a value for T_C for the grid box was available. When T_C was available, and it was > 0.35 , the direct flux at the surface, F_{Sdir} , was computed as

$$F_{Sdir} = F_{SD} (T_C \square 0.35), \quad (47)$$

and the diffuse flux at the surface, F_{Sdif} , as

$$F_{Sdif} = F_{SD} (1.35 \square T_C). \quad (48)$$

Together, these equations mean that for clear skies ($T_C = 1.0$), direct flux is 65% of the global flux, and the remaining 35% is diffuse flux. Further, when $T_C \square 0.35$ (generally dense cloudiness), the direct flux is reduced to zero and the entire global flux is in the diffuse form. Staylor almost always devised an approximate method when a variable required to complete the calculation was not available from its standard sources. In keeping with that approach, Staylor adopted the 65/35 partitioning (the same as for clear skies) when a value of T_C could not be determined from the usual methods. Exact details on how

Staylor derived Eqs. (47) and (48) were not available, but the authors believe that these equations were developed by fitting curves to the results obtained by Pinker and Laszlo (1992a). An effort to verify the above partitioning (Whitlock and LeCroy, unpublished results) showed the 65/35 ratio to be a good estimate for average atmospheric conditions. The PAR at the surface, F_{SPAR} , was computed as

$$F_{SPAR} = F_{SD} \left\{ 0.42 + 2(u - 0.5)^2 \right\}, \quad (49)$$

for both clear and cloudy conditions. It is believed that Eq. (49) was developed by fitting curves to the results derived by Pinker and Laszlo (1992b).

4. Input data sources

The most extensive prior application of this algorithm was for the 8-year period (July 1983 to June 1991) for which monthly average global SRB fields have been published (Gupta et al. 1999). All required cloud parameters, column precipitable water (PW), and column ozone for that work were taken from the ISCCP-C1 datasets. The latter two, namely, PW and column ozone were TOVS products incorporated into ISCCP-C1 datasets. Surface albedos were derived from literature formulas and from ERBE clear-sky TOA albedos, as discussed in Sec. 3.4. Aerosol properties used were climatological average values for four standard aerosol types, namely, maritime, continental, desert, and snow/ice (Deepak and Gerber 1983). The surface was classified as one of five types, namely, ocean, coast, land, desert, and snow/ice. A single aerosol type, or a combination of two, was associated with each of the surface types as described in Appendix C. Flux computations were made on a grid-box basis for the 6596-box equal-area grid which has a resolution of about 280 km x 280 km.

The state-of-the-art for some of the above datasets has advanced considerably over the last few years, and newer datasets are being used for the current applications. Cloud properties used in the current work are derived from pixel level ISCCP data, known as the DX data (Stackhouse et al. 2001) with the same algorithms as used for deriving the ISCCP-D products. Further, these cloud properties are being derived on an equal-area global grid, which consists of 44016 boxes and is called the nested grid. Areas of the boxes of this grid approximately equal the area of a $1^\circ \times 1^\circ$ box at the equator. The increased spatial resolution provides insights into the structure of clouds not achievable with C1 or D1 datasets. Column PW for the current work is being derived from the data assimilation model products of the Goddard Earth Observing System, version-1 (GEOS-1; Schubert et al. 1993), produced by the Data Assimilation Office (DAO) at the NASA Goddard Space Flight Center (GSFC). The GEOS-1 column PW is produced 6-hourly, and thus contains a representation of the diurnal variability. By contrast, the ISCCP-C1 column PW was a once/day product from TOVS, and contained no diurnal variability. Column ozone used for the current work comes from a long record available from the Total Ozone Mapping Spectrometer (TOMS), which flew aboard Nimbus-7 and Meteor-3, and is presently flying aboard EP-TOMS. The TOMS ozone product is deemed to be considerably superior to the ISCCP-C1 column ozone, which is a TOVS product derived from an infrared channel on the HIRS-2 instruments. Column PW from GEOS-1 and TOMS ozone were both regridded to the nested grid to ensure compatibility with the new cloud products. Surface albedos and aerosol properties are still obtained from the same sources as in the earlier work. A value of 1365 Wm^{-2} for the solar constant, based on ERBE measurements was used in the earlier work, and is also being used for the current work.

Table 1. Inputs required for LPSA and data sources used in the past, for the present work, and expected to be used in the future.

LPSA input	<u>Data sources</u>		
	Past	Present	Future
Solar constant	ERBE	ERBE	TBD
TOA reflected radiances	ISCCP – C1	ISCCP - DX	ISCCP - DX
Cloud amount	ISCCP – C1	ISCCP – DX	ISCCP - DX
Cloud optical depth	ISCCP – C1	ISCCP – DX	ISCCP - DX
Column PW	TOVS	GEOS - 1	GEOS - 3
Surface albedo	LF, ERBE	LF, ERBE	TBD
Column ozone	TOVS	TOMS	TOMS
Aerosol properties	D&G	D&G	TBD

Key: TBD - To be determined; LF – Literature formulas; D&G – Deepak and Gerber (1983).

Datasets of still better quality are continuously coming online and will be used as they become available. For example, column PW for future work is likely to come from GEOS-3 or later versions of the data assimilation model now in use at the DAO. Newer models of aerosol spatial and temporal distribution and their optical properties are being explored for use in future work, as are the newer sources of surface albedo. TOMS is likely to continue as the future source of column ozone. Values of solar constant obtained from newer measurements will be examined to ascertain if their use in place of the ERBE-based value is warranted. A concise summary of the past, present, and future input data sources for LPSA is presented in Table 1.

5. Results and discussion

The current version of LPSA and the input datasets described in Sec. 4 have been used to derive a number of surface SW parameters for all months of 1986 and 1992. A complete list of these parameters is given below:

1. Clear-sky insolation,
2. All-sky insolation,
3. All-sky net SW flux,
4. Direct SW flux,
5. Diffuse SW flux,
6. Photosynthetically active radiation, and
7. All-sky surface albedo.

Since the primary purpose of this report is to explain and document the scientific basis of the algorithm as much as possible, only small samples of these results will be presented and discussed here. Detailed presentations and discussions may be undertaken in the future when such results are produced in the context of various research projects. It suffices here to show that the results are physically consistent with the input meteorological fields used and with similar results from earlier work. With those objectives in mind, all-sky insolation results for 1992 are highlighted in this report. All-sky insolation is the most widely measured and used surface SW parameter. Also, the 1992 results are completely new for

this algorithm, being outside the July 1983 – June 1991 period, for which similar results were derived using ISCCP-C1 data for inputs (Gupta et al. 1999). The results for 1992 are compared with results for 1986, both derived using the current version of the algorithm. This comparison may provide an estimate of interannual differences between 1986 and 1992, if any, as both sets are derived using identical input sources. Also, current 1986 results are compared with corresponding results derived earlier using the same algorithm but with ISCCP-C1 inputs. The latter comparison provides an estimate of the differences arising from (i) DX vs. C1 cloud inputs, (ii) GEOS-1 vs. TOVS meteorological inputs, and (iii) TOMS vs. TOVS ozone.

Table 2. Comparison of hemispheric and global average all-sky surface insolation (Wm^{-2}) for January, July, and the whole year for 1992 and 1986 from current work, and for 1986 from earlier work with ISCCP-C1 inputs.

	N. H.	S. H.	Global
1992 – Current Work			
Jan.	128.5	256.0	192.3
Jul.	245.2	116.6	180.9
Ann.	191.2	185.2	188.2
1986 – Current Work			
Jan.	127.2	246.7	186.9
Jul.	243.6	115.4	179.5
Ann.	189.8	184.4	187.1
1986 – From ISCCP-C1			
Jan.	126.8	249.7	188.2
Jul.	241.7	118.0	179.8
Ann.	186.6	182.9	184.8

Figure 1 shows the seasonal variability of all-sky surface insolation averaged over the hemispheres and the globe for 1992 and the two datasets for 1986. All plots show a strong seasonal variability for the hemispheric averages, and a weak one for the global average. Table 2 presents numbers based on the same datasets for hemispheric and global averages for January, July, and the whole year. Seasonal variability (January to July difference) for the SH shows a slightly larger magnitude than for the NH. This difference arises from two reinforcing causes. First, the Sun-Earth distance is minimum during January (SH summer) and maximum during July, providing a stronger seasonal contrast over the SH. Second, there is a large seasonal variability of column water vapor in the NH, with a strong maximum in July (NH summer), which lowers the seasonal contrast for the NH. The numbers in Table 2 seem to indicate interannual differences between the 1992 and 1986 results from the current work, and those arising from the use of different input sources between the two datasets for 1986. It is emphasized that the above differences are presented only for illustrative purposes, and are not meant to establish interannual variability of surface insolation or characteristics of the input data sources.

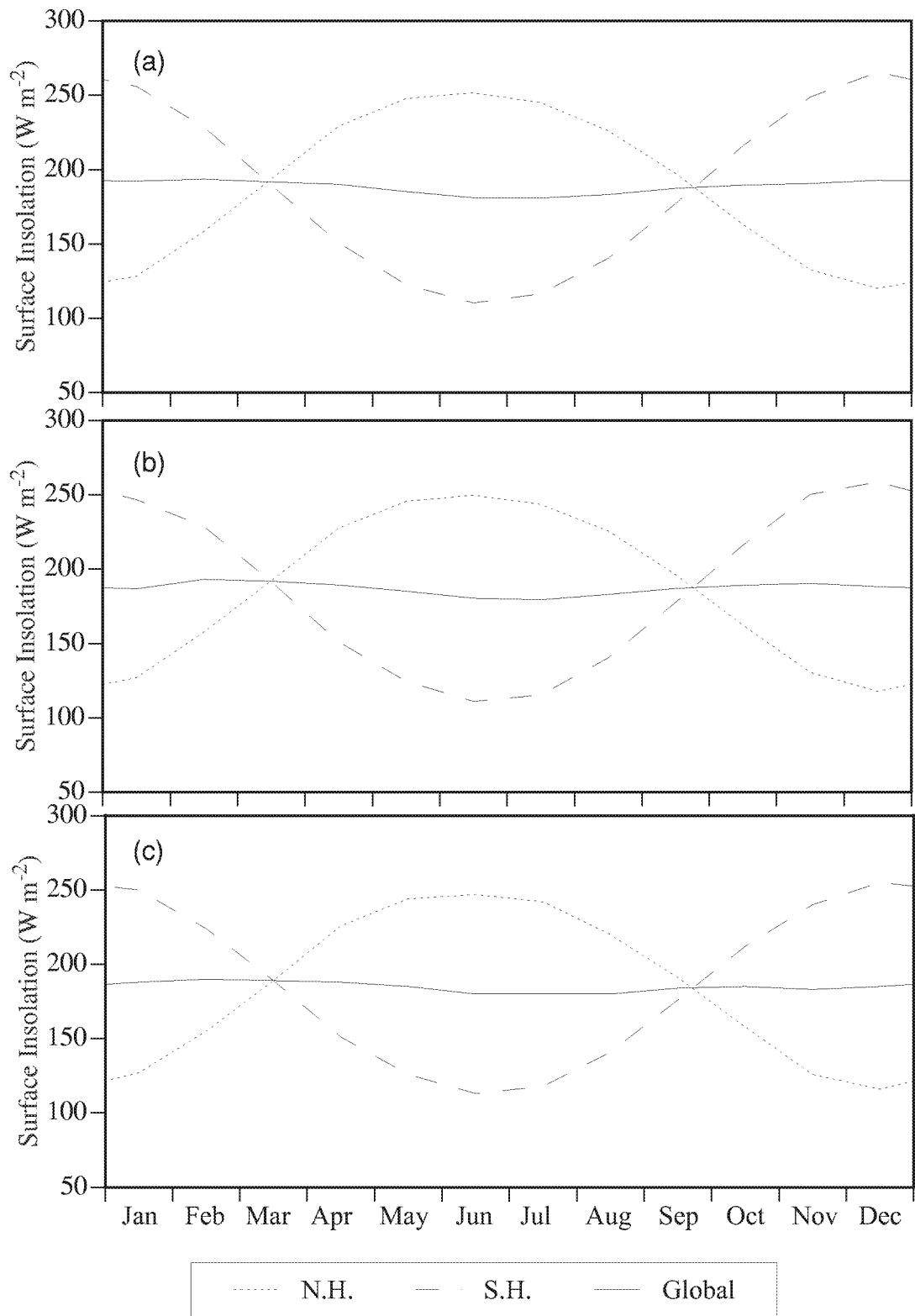
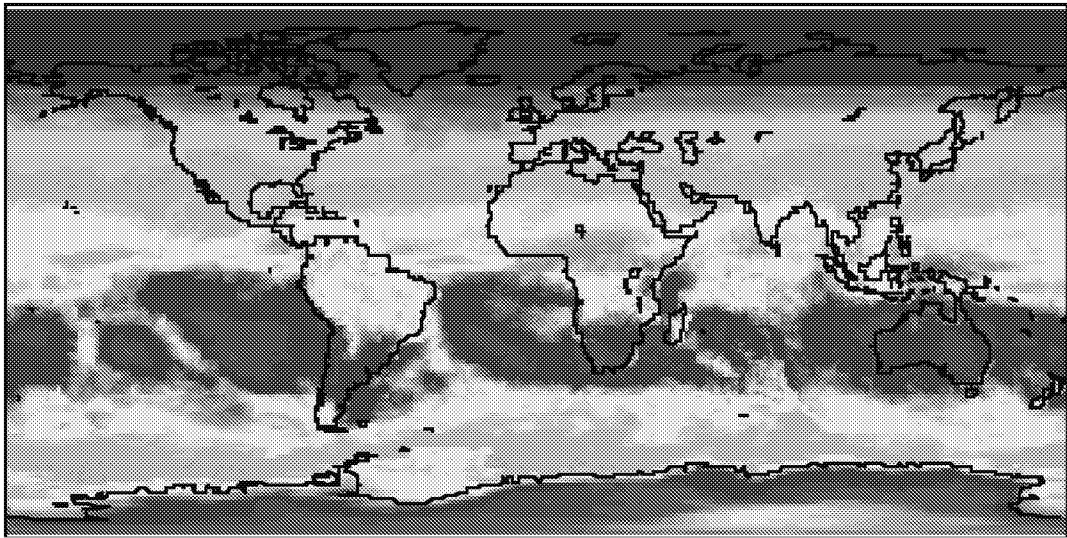
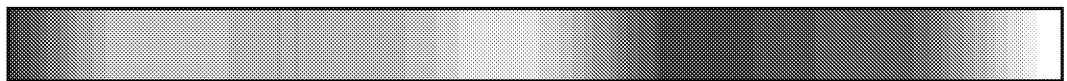
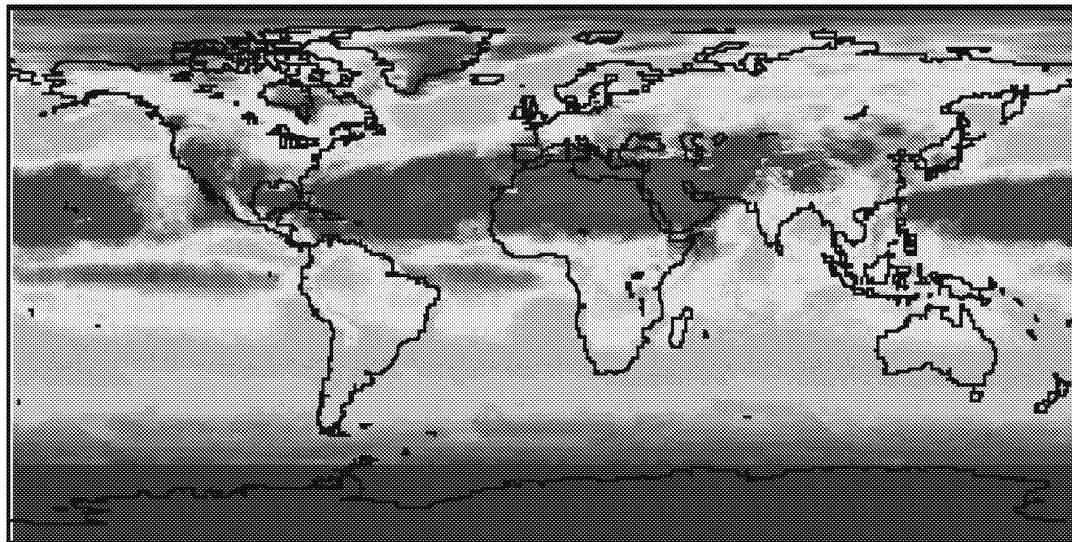


Figure 1. Time series of hemispheric and global averages of surface insolation for (a) 1992 from current work, (b) 1986 from current work, and (c) 1986 derived for ISCCP-C1 inputs.

January 1992



July 1992



0 50 100 150 200 250 300 350 400 450

Figure 2. Geographical distribution of monthly average surface insolation (W m^{-2}) for January and July 1992 derived with inputs used in the current work.

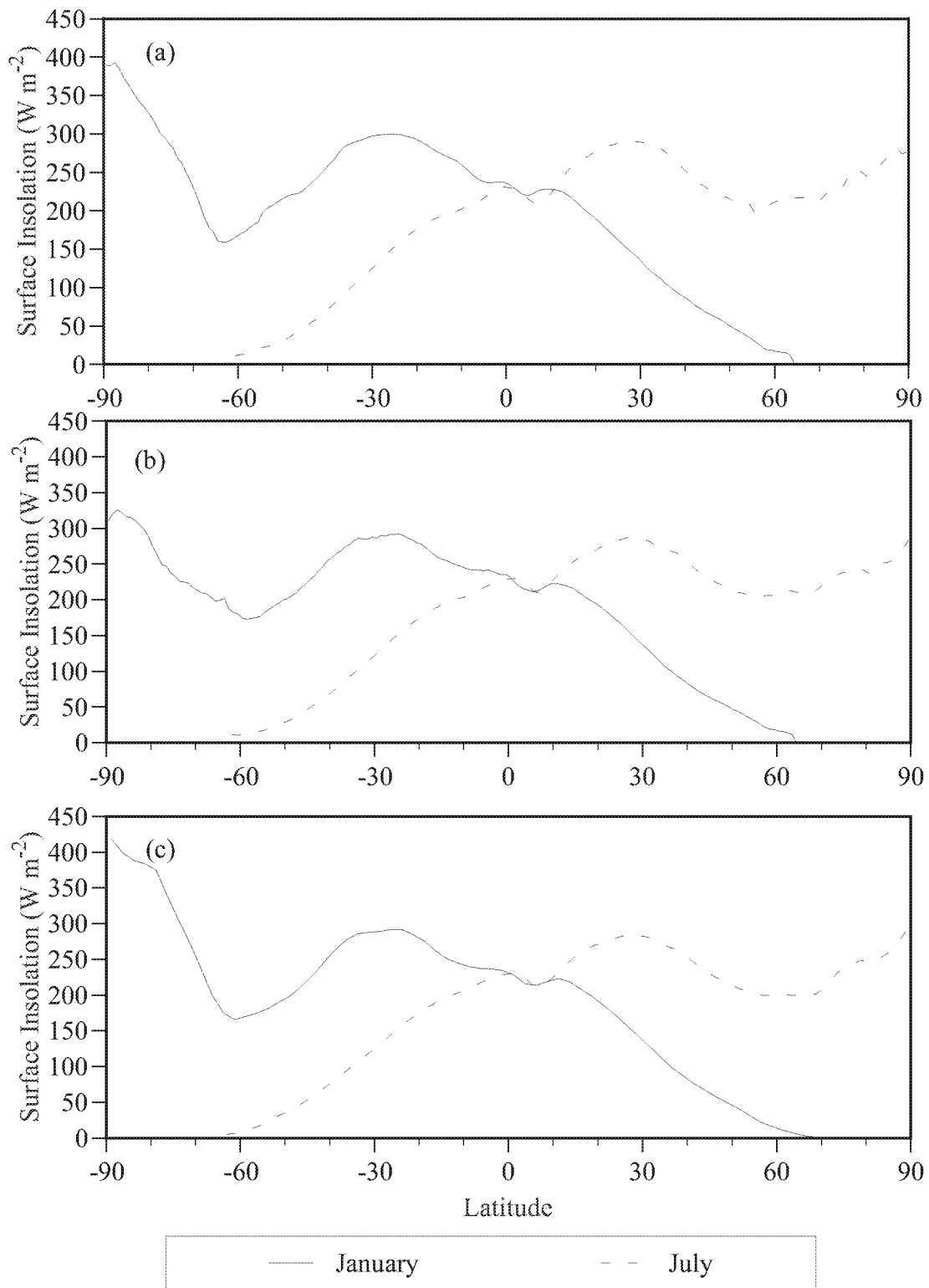


Figure 3. Zonally-averaged surface insolation for January and July for (a) 1992 from current work, (b) 1986 from current work, and (c) 1986 derived for ISCCP-C1 inputs.

Figure 2 shows the geographical distribution of monthly average surface insolation for January and July 1992. The highest values occur over subtropical subsidence regions and polar areas of the summer hemisphere. Small cloud amounts over subsidence regions and longer sunshine duration over polar areas account for these features. Large cloud amounts in the storm tracks account for the much lower values over midlatitudes of the summer hemisphere. For the winter hemisphere, polar areas do not receive sunlight, and the low values over midlatitudes result from a combination of low TOA insolation and dense cloud cover in the storm tracks. Relatively low values over the equatorial regions are caused by the heavy cloudiness along the intertropical convergence zone (ITCZ).

Figure 3(a) shows zonally-averaged surface insolation for January and July derived from the same 1992 dataset. Figures 3(b) & 3(c) show corresponding results from the two datasets for 1986. The only significant differences between the three panels are seen in the January curves poleward of 60° in the SH. Qualitative comparisons of the input parameters used for computing these insolation fields showed that these differences arise primarily from corresponding differences in the cloud fields. Cloud amounts between 60° S and the South Pole in the 1986 dataset used in the current work were significantly higher than for the other two datasets. The results presented above demonstrate that the fields of SW parameters derived in the current work are physically understandable and consistent with the results of earlier work.

A high degree of confidence in the quality of all-sky surface insolation shown above notwithstanding, a note of caution is in order regarding the quality of the direct, diffuse, and PAR fluxes derived with this algorithm. The formulas used to derive these products appear highly empirical and the results have never been validated. For these reasons, the direct, diffuse, and PAR fluxes were never distributed to the science community in the past, and will not be distributed in the near future. The inclusion of Eqs. (47) – (49) in this report was driven by the desire to present all elements of the algorithm as proposed by Staylor. The authors do not recommend the use of these formulas by the readers without independent validation.

6. Planned enhancements

A number of steps are being undertaken to update and enhance this algorithm to prepare it for newer applications. The first of these will be to change the time resolution from daily to instantaneous so that the results can be compared with high temporal resolution surface observations. The next will be to examine each of the attenuation terms in Eq. (23), including the models and measurements on which those terms are based. New parameterizations of the attenuation processes are currently under development by the authors and will be incorporated into this algorithm after they are validated. Newer models of aerosol spatial and temporal distribution and their optical properties are being explored as are newer sources of surface albedo. Those too will be incorporated into the algorithm when available. It is also planned to undertake a critical examination of Eqs. (47) – (49) which are used for computing direct, diffuse, and PAR fluxes respectively. Results of these equations will be compared with other model results and observations, and the equations will be modified as necessary.

References

- Barkstrom, B. R., E. F. Harrison, G. L. Smith, R. N. Green, J. F. Kibler, R. D. Cess, and the ERBE Science Team, 1989: Earth Radiation Budget Experiment archival and April 1985 results. *Bull. Amer. Meteor. Soc.*, **70**, 1254-1262.
- Chen, T. S., and G. Ohring, 1984: On the relationship between clear-sky planetary and surface albedos. *J. Atmos. Sci.*, **41**, 156-158.
- Chou, M. -D., and M. J. Suarez, 1999: A solar radiation parameterization for atmospheric studies. NASA TM-104606, **15**, 40 pp.
- Darnell, W. L., W. F. Staylor, S. K. Gupta, and F. M. Denn, 1988: Estimation of surface insolation using Sun-synchronous satellite data. *J. Climate*, **1**, 820-835.
- Darnell, W. L., W. F. Staylor, S. K. Gupta, N. A. Ritchey, and A. C. Wilber, 1992: Seasonal variation of surface radiation budget derived from ISCCP-C1 data. *J. Geophys. Res.*, **97**, 15 741-15 760.
- Deepak, A., and H. E. Gerber, Eds., 1983: Report of the experts meeting on aerosols and their climatic effects. WCP-55, 107 pp.
- Gupta, S. K., N. A. Ritchey, A. C. Wilber, C. H. Whitlock, G. G. Gibson, and P. W. Stackhouse Jr., 1999: A climatology of surface radiation budget derived from satellite data. *J. Climate*, **12**, 2691-2710.
- Hoyt, D. V., 1978: A model for the calculation of solar global insolation. *Solar Energy*, **21**, 27-35.
- Iqbal, M., 1983: *An Introduction to Solar Radiation*. Academic Press. 390 pp.
- Koepke, P., and K. T. Kriebel, 1987: Improvements in the shortwave cloud-free radiation budget accuracy. Part I: Numerical study including surface anisotropy. *J. Climate Appl. Meteor.*, **26**, 374-395.
- Kondratyev, K. Ya., 1973: *Radiation characteristics of the atmosphere and the Earth's surface*. NASA TT-F-678, 580 pp.
- Lacis, A., and J. E. Hansen, 1974: A parameterization for the absorption of solar radiation in the Earth's atmosphere. *J. Atmos. Sci.*, **31**, 118-133.
- Li, Z., H. G. Leighton, and R. D. Cess, 1993: Surface net solar radiation estimated from satellite measurements: Comparisons with tower observations. *J. Climate*, **6**, 1764-1772.
- Manabe, S., and R. F. Strickler, 1964: Thermal equilibrium of the atmosphere with a convective adjustment. *J. Atmos. Sci.*, **21**, 361-385.
- Moser, W., and E. Raschke, 1984: Incident solar radiation over Europe estimated from METEOSAT data. *J. Climate Appl. Meteor.*, **23**, 166-170.
- Payne, R. E., 1972: Albedo of the sea surface. *J. Atmos. Sci.*, **29**, 959-970.
- Peixoto, J. P., and A. H. Oort, 1993: *Physics of Climate*, American Institute of Physics, 520 pp.

- Pinker, R., and I. Laszlo, 1992a: Modeling surface solar irradiance for satellite applications on a global scale. *J. Appl. Meteor.*, **31**, 194-211.
- Pinker, R., and I. Laszlo, 1992b: Global distribution of photosynthetically active radiation as observed from satellites. *J. Climate*, **5**, 56-65.
- Ramanathan, V., 1986: Scientific use of surface radiation budget for climate studies. In *Surface Radiation Budget for Climate Applications*, J. T. Suttles and G. Ohring, Eds., NASA RP-1169, 58-86.
- Rossow, W. B., and R. A. Schiffer, 1991: ISCCP cloud data products. *Bull. Amer. Meteor. Soc.*, **72**, 2-20.
- Sellers, W. D., 1965: *Physical Climatology*, The University of Chicago Press, 272 pp.
- Schubert, S. D., R. B. Rood, and J. Pfaendtner, 1993: An assimilated dataset for Earth science applications. *Bull. Amer. Meteor. Soc.*, **74**, 2331-2342.
- Spencer, J. W., 1971: Fourier series representation of the position of the Sun. *Search*, **2**, 172.
- Stackhouse, P. W., S. K. Gupta, S. J. Cox, M. Chiacchio, and J. C. Mikovitz, 2000: The WCRP/GEWEX Surface Radiation Budget Project Release 2: An assessment of surface fluxes at 1 degree resolution. In *IRS 2000: Current Problems in Atmospheric Radiation*, W. L. Smith and Y. M. Timofeyev, Eds., *International Radiation Symposium*, St. Petersburg, Russia, July 24-29, 2000.
- Staylor, W. F., 1985: Reflection and emission models for clouds derived from Nimbus 7 Earth radiation budget scanner measurements. *J. Geophys. Res.*, **90**, 8075-8079.
- Staylor, W. F., W. L. Darnell, and S. K. Gupta, 1983: Estimation of clear-sky insolation using satellite and ground meteorological data. Preprints, *Fifth Conference on Atmospheric Radiation*, Baltimore, MD, Amer. Meteor. Soc., 440-443.
- Staylor, W. F., and A. C. Wilber, 1990: Global surface albedos estimated from ERBE data. Preprints, *Seventh Conference on Atmospheric Radiation*, San Francisco, CA, Amer. Meteor. Soc., 231-236.
- Suttles, J. T., and G. Ohring, 1986: Surface radiation budget for climate applications. *NASA Reference Publication 1169*, NASA, Washington, DC, 132pp.
- Wiscombe, W. J., and G. W. Grams, 1976: The backscattered fraction in two-stream approximations. *J. Atmos. Sci.*, **33**, 2440-2451.
- WCRP-69, 1992: Radiation and Climate: Report of the fourth session of the WCRP working group on radiative fluxes. *WMO/TD-No. 471*.
- Yamamoto, G., 1962: Direct absorption of solar radiation by atmospheric water vapor, carbon dioxide and molecular oxygen. *J. Atmos. Sci.*, **19**, 182-188.

Appendix A

Astronomical Relationships

The insolation reaching the Earth is governed by the inverse square law through the eccentricity correction factor, $(d_m/d)^2$, in Eq. (2). The mean Sun-Earth distance, d_m , is 1.496×10^{11} m and is called an astronomical unit (AU). The instantaneous Sun-Earth distance varies from 1.471×10^{11} m (0.983 AU) in early January to 1.521×10^{11} m (1.017 AU) in early July. Iqbal (1983) presents several simple expressions for the daily average value of $(d_m/d)^2$ and recommends one derived by Spencer (1971):

$$\begin{aligned} (d_m/d)^2 = & 1.000110 + 0.034221 \cos \Gamma + 0.001280 \sin \Gamma \\ & + 0.000719 \cos 2\Gamma + 0.000077 \sin 2\Gamma, \end{aligned} \quad (\text{A1})$$

where Γ (in radians) is given by

$$\Gamma = 2\pi(d_n - 1)/365, \quad (\text{A2})$$

for a year of 365 days. Equations (A1) and (A2) were used in the present work with 366 substituted in Eq. (A2) for the leap years. According to Iqbal (1983), the maximum error in $(d_m/d)^2$ computed with Eq. (A1) is 0.0001.

Another astronomical variable which affects insolation reaching the Earth is the solar declination, δ , through $\cos Z$ in Eq. (3). Solar declination varies from $+23.5^\circ$ at the summer solstice (about 21 June) to -23.5° at the winter solstice (about 22 December) and goes through zero at the vernal and autumnal equinoxes (about 21 March and 22 September, respectively). Note that the above seasonal descriptions apply to the NH; the opposite apply to the SH. Iqbal (1983) presents several expressions for the daily average value of δ and recommends one, also derived by Spencer (1971):

$$\begin{aligned} \delta = & (0.006918 - 0.399912 \cos \Gamma + 0.070257 \sin \Gamma \\ & - 0.006758 \cos 2\Gamma + 0.000907 \sin 2\Gamma \\ & - 0.002697 \cos 3\Gamma + 0.00148 \sin 3\Gamma)(180/\pi), \end{aligned} \quad (\text{A3})$$

where Γ is already defined in Eq. (A2). Equation (A3) was used in the present work. According to Iqbal (1983), the maximum error in δ computed with Eq. (A3) is 0.0006 radian.

Appendix B

Attenuation Under Clear Skies

The absorption/scattering processes of the various constituents (excluding aerosols) contributing to the attenuation of solar radiation in the atmosphere are represented by Eqs. (24) – (28) for an overhead Sun. As stated in Sec. 3.2, equations in these exact forms were not found in the cited references, namely, Lacis and Hansen (1974), and Yamamoto (1962). However, functionally equivalent equations representing attenuation due to water vapor, ozone, and Rayleigh scattering are given in the Lacis and Hansen reference. Comparisons of Eqs. (24) and (25) with corresponding formulas from Lacis and Hansen are presented below in Figs. B1 and B2 respectively. Figure B1 shows good agreement for column water vapor values above 0.1 pr-cm which makes the use of Eq. (24) appropriate over most of the globe. Figure B2 shows good agreement throughout the range.

Absorption due to CO_2 and O_2 (Eqs. 26 and 27) is related to surface pressure, P_s . At sea level ($P_s = 1$), attenuation by CO_2 amounts to about 0.63% of the TOA insolation which is close to that obtained from the curves for CO_2 absorption given by Manabe and Strickler (1964). Absorption by O_2 amounts to about 0.75%. This value agrees well with those obtained from: i) the Hoyt (1978) formula, ii) the parameterization by Chou and Suarez (1999), and iii) line-by-line calculations made by the authors (unpublished results). Attenuation due to molecular scattering (Eq. 28) amounts to about 3.5% of the TOA insolation. This number is in close agreement with that obtained from Eq. (41) of Lacis and Hansen which represents atmospheric albedo due to Rayleigh scattering. Also, it is important to note that Eq. (28) represents only the upward part of the scattered radiation. The downward part remains in the downward radiation stream.

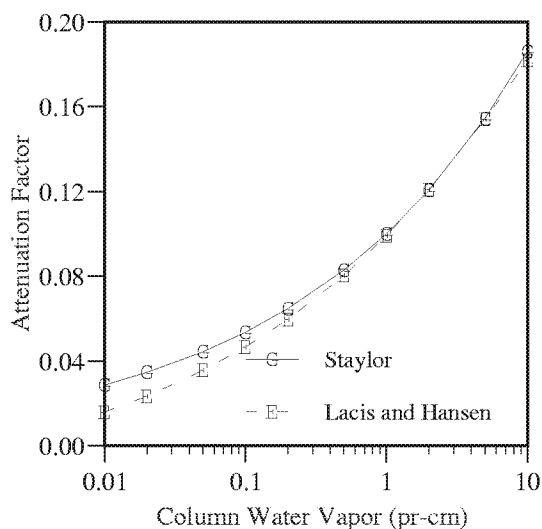


Figure B1. Attenuation by water vapor.

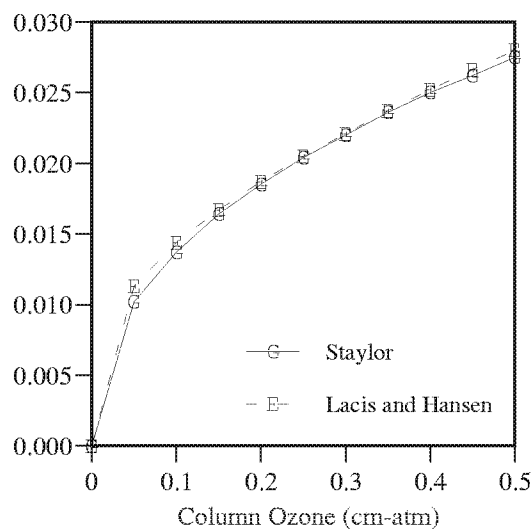


Figure B2. Attenuation by ozone

Appendix C

Aerosol Distribution and Radiative Properties

The magnitude of the aerosol attenuation in this model was computed on the basis of five surface scene types listed in Table C1. Standard aerosol types (e.g., maritime, continental, desert) and values of $\bar{\alpha}_0$, and g for them were adopted from Deepak and Gerber (1983) with minor adjustments. A standard aerosol type (or a combination of them) was associated with each surface scene type. In addition, climatological mean values of $\bar{\alpha}_{aer}$, further parameterized by Staylor in terms of μ for each surface scene type, were used. All of this information is presented in Table C1 below.

Table C1. Aerosol radiative parameters $\bar{\alpha}_{aer}$, $\bar{\alpha}_0$, and g for the five surface scene types. A_{Tclr} in the formula for $\bar{\alpha}_{aer}$ is the ERBE clear-sky TOA albedo.

Scene type	Aerosol type	$\bar{\alpha}_{aer}$	$\bar{\alpha}_0$	g
Ocean	Maritime	0.15μ	0.98	0.60
Land	Continental	0.35μ	0.90	0.66
Desert	Desert	$(0.3+0.5A_{Tclr})\mu$	0.92	0.60
Coast	50/50 Maritime & Continental	0.25μ	0.94	0.64
Snow/Ice	Snow/Ice	0.03	0.97	0.67

Appendix D

Sampling Procedures and Alternative T_C Computations

The regression coefficients C_1 and C_2 (Eq. 35) for computing overcast reflectance, R_{ovc} , for each grid box and each day were determined by linear regression between $R_{ovc}\mu\mu_o$ and $[\mu\mu_o/(\mu+\mu_o)]^2$. Regression was performed separately for each ISCCP satellite for every month. Only overcast grid boxes for which solar and view zenith angles were less than 70° were sampled for regression. This procedure still left datasets of more than 100,000 grid boxes, a size that was considered too cumbersome for regression analysis. These were reduced to a more manageable size (less than 10,000) by sorting $R_{ovc}\mu\mu_o$ and $[\mu\mu_o/(\mu+\mu_o)]^2$ on cloud optical depth and retaining only those in the highest 10 – 20% of optical depth range.

Corresponding coefficients for computing clear-sky reflectance, R_{clr} , over ice-free oceans (C_3 and C_4 in Eq. 36) were determined by linear regression between R_{clr} and $(\mu\mu_o)^{0.75}$. Clear grid boxes, subject to the same restrictions of solar and view zenith angles as above, were sampled for this regression. Many of these datasets also had more than 40,000 values, still too large for regression analysis. These datasets were randomly sampled to reduce the number down to about 4,000.

Two conditions encountered under which the use of Eq. (34) was deemed inappropriate for T_C computation were the following:

- 1) When $(R_{ovc} - R_{clr})$ was too small. A lower limit of 0.15 was imposed on $(R_{ovc} - R_{clr})$.
- 2) When $(R_{ovc} - R_{meas})$ was negative. Under these conditions, when both cloud amount and cloud optical depth were available, T_C was computed as

$$T_C = 0.05 + 0.95 (1 - 0.2 A_C \tau_C^{0.37}), \quad (D1)$$

where A_C is the fractional cloud amount and τ_C is the cloud optical depth. When only A_C was available, T_C was computed as

$$T_C = 0.2 + 0.8 (1 - A_C)^{0.7}. \quad (D2)$$

Both equations provide $T_C = 1$ for $A_C = 0$ (clear sky). For $A_C = 1$ (overcast), Eq. (D1) provides the minimum value of T_C ($= 0.05$) for a τ_C value of about 80. This was assumed to be the highest average value τ_C for a dense overcast. Also for $A_C = 1$, Eq. (D2) provides $T_C = 0.2$, which in terms of Eq. (D1) corresponds to a value of τ_C of about 50.

Appendix E

Alternative Surface Albedo Computations

As stated in Sec. 3.4, when snow/ice cover was present in a grid box, alternative methods were used for computing A_{Sclr} and A_{Sovc} as follows:

Oceans: When an ERBE-derived value of A_{Sclr} was available, it was used as such and a corresponding value of A_{Sovc} was computed as

$$A_{Sovc} = A_{Sclr} (u/0.6)^{(1/s)}, \quad (E1)$$

where s represents the fractional snow/ice cover for the grid box. When A_{Sclr} from ERBE was not available, it was computed as

$$A_{Sclr} = A_{St} (1 - s) + 0.5 s, \quad (E2)$$

where A_{St} represents a value computed from Eq. (39) but capped at 0.25. The corresponding value of A_{Sovc} was computed as

$$A_{Sovc} = 0.065 (1 - s) + 0.5 s. \quad (E3)$$

Eq. (E2) reduces to Eq. (39) when $s = 0$ (ice-free ocean) but caps the value of A_{Sclr} at 0.25, and Eq. (E3) reduces to Eq. (40). Both (E2) and (E3) cap surface albedo values at 0.50 when $s = 1$.

Other surfaces: When snow/ice cover is present in a grid box and an ERBE-derived value of surface albedo is available, that value is used for both A_{Sclr} and A_{Sovc} . When an ERBE-derived value is not available, A_{Sclr} is computed as

$$A_{Sclr} = 0.2 (1 - s) + 0.7 s, \quad (E4)$$

and the same value is used for A_{Sovc} .

REPORT DOCUMENTATION PAGE			Form Approved OMB No. 0704-0188
Public reporting burden for this collection of information is estimated to average 1 hour per response, including the time for reviewing instructions, searching existing data sources, gathering and maintaining the data needed, and completing and reviewing the collection of information. Send comments regarding this burden estimate or any other aspect of this collection of information, including suggestions for reducing this burden, to Washington Headquarters Services, Directorate for Information Operations and Reports, 1215 Jefferson Davis Highway, Suite 1204, Arlington, VA 22202-4302, and to the Office of Management and Budget, Paperwork Reduction Project (0704-0188), Washington, DC 20503.			
1. AGENCY USE ONLY (Leave blank)	2. REPORT DATE December 2001	3. REPORT TYPE AND DATES COVERED Technical Publication	
4. TITLE AND SUBTITLE The Langley Parameterized Shortwave Algorithm (LPSA) for Surface Radiation Budget Studies Version 1.0		5. FUNDING NUMBERS WU 229-01-02-10	
6. AUTHOR(S) Shashi K. Gupta, David P. Kratz, Paul W. Stackhouse, Jr., and Anne C. Wilber			
7. PERFORMING ORGANIZATION NAME(S) AND ADDRESS(ES) NASA Langley Research Center Hampton, VA 23681-2199		8. PERFORMING ORGANIZATION REPORT NUMBER L-18139	
9. SPONSORING/MONITORING AGENCY NAME(S) AND ADDRESS(ES) National Aeronautics and Space Administration Washington, DC 20546-0001		10. SPONSORING/MONITORING AGENCY REPORT NUMBER NASA/TP-2001-211272	
11. SUPPLEMENTARY NOTES Gupta and Wilber: Analytical Services and Materials, Inc., Hampton, VA; Kratz and Stackhouse: Langley Research Center, Hampton, VA			
12a. DISTRIBUTION/AVAILABILITY STATEMENT Unclassified-Unlimited Subject Category 47 Distribution: Standard Availability: NASA CASI (301) 621-0390		12b. DISTRIBUTION CODE	
13. ABSTRACT (Maximum 200 words) An efficient algorithm was developed during the late 1980's and early 1990's by W. F. Staylor at NASA/LaRC for the purpose of deriving shortwave surface radiation budget parameters on a global scale. While the algorithm produced results in good agreement with observations, the lack of proper documentation resulted in a weak acceptance by the science community. The primary purpose of this report is to develop detailed documentation of the algorithm. In the process, the algorithm was modified whenever discrepancies were found between the algorithm and its referenced literature sources. In some instances, assumptions made in the algorithm could not be justified and were replaced with those that were justifiable. The algorithm uses satellite and operational meteorological data for inputs. Most of the original data sources have been replaced by more recent, higher quality data sources, and fluxes are now computed on a higher spatial resolution. Many more changes to the basic radiation scheme and meteorological inputs have been proposed to improve the algorithm and make the product more useful for new research projects. Because of the many changes already in place and more planned for the future, the algorithm has been renamed the Langley Parameterized Shortwave Algorithm (LPSA).			
14. SUBJECT TERMS Radiation Budget, Surface Radiation, Shortwave Algorithms Parameterizations, CERES, GEWEX/SRB		15. NUMBER OF PAGES 31	16. PRICE CODE A03
17. SECURITY CLASSIFICATION OF REPORT Unclassified	18. SECURITY CLASSIFICATION OF THIS PAGE Unclassified	19. SECURITY CLASSIFICATION OF ABSTRACT Unclassified	20. LIMITATION OF ABSTRACT UL